Interaction between elastic waves and prismatic dislocation loops

Natalia Rodríguez,[1] Agnès Maurel,[2,a)] Vincent Pagneux,[3] Felipe Barra,[4] and Fernando Lund[4,1]
[1]*Departamento de Ingeniería Mecánica, Facultad de Ciencias Físicas y Matemáticas, Universidad de Chile, Santiago, Chile*
[2]*Laboratoire Ondes et Acoustique, UMR CNRS 7587, Ecole Supérieure de Physique et Chimie Industrielles, 10 Rue Vauquelin, 75005 Paris, France*
[3]*Laboratoire d'Acoustique de l'Université de Maine, UMR CNRS 6613, Avenue Olivier Messiaen, 72085 Le Mans Cedex 9, France*
[4]*Departamento de Física and CIMAT, Facultad de Ciencias Físicas y Matemáticas, Universidad de Chile, Casilla 487-3, Santiago, Chile*

(Received 23 December 2008; accepted 5 August 2009; published online 15 September 2009)

The properties of prismatic dislocation loops, generated by radiation in metals, have remained elusive for decades, and recent advances in computational capabilities as well as transmission electron microscopy have renewed interest in their study. Acoustic and elastic waves could become an interesting, nonintrusive, probe to this end, as they have for other dislocation configurations. What then are the characteristics of elastic wave scattering that would be sensitive to a prismatic loop signature? In this paper, we report the scattering cross section for an elastic wave by a prismatic dislocation loop. It differs in significant ways from the analog quantity in the case of pinned dislocation segments, the most significant being the polarization of the scattered wave. The properties of a coherent wave traveling through an elastic medium filled with randomly placed and randomly oriented such loops are also reported. At long wavelengths, the effective wave velocity and attenuation coefficients resemble those for a similar case with pinned dislocation segments.
 [doi:10.1063/1.3213338]

I. INTRODUCTION

A series of recent papers[1–8] has revisited the issue of the interaction of elastic waves with dislocations in continuous media. The interaction with a single dislocation in two[1–3,6] and three dimensions, both in an infinite[4] and a semi-infinite[7] medium, has been studied in detail. Results for an infinite medium have provided information (such as polarization, angular dependence, and near and far field behaviors) on the interaction of elastic waves with dislocations, not available through the classic Granato–Lücke theory,[9,10] which is a scalar mean field theory. Results for a semi-infinite medium[7] have shed new light on recent experiments using x-ray topography imaging of surface acoustic waves interacting with subsurface dislocations in $LiNbO_3$.[11] Interaction with many dislocations within the framework of multiple scattering theory[5] has provided a generalization of the Granato–Lücke theory[9,10] that accounts for the vector nature of both the elastic waves and the string that mimics the dislocation. With this generalization, it became possible to explain quantitatively the different attenuations of longitudinal and transverse waves measured in a number of materials.[12] Application of the theory to low angle grain boundaries[8] has explained the frequency behavior of acoustic attenuation in polycrystals.[13] For a review, see Ref. 14.

One of the motivations for the program described in the previous paragraph has been to develop nonintrusive tools to characterize plasticity in metals through the acoustic probing of dislocation properties. Recent resonant acoustic spectroscopy (RUS) experiments that measure dislocation densities in aluminum provide strong encouragement for this program,[15] and in order to continue toward this end, it is needed to discriminate between the various possible sources of scattering, as well as among the possible dislocation configurations.

A dislocation configuration that has attracted considerable interest recently is the prismatic dislocation loop (PMDL), a dislocation loop that has a Burgers vector normal to its plane. PMDLs have long been observed to arise in metals subject to radiation.[16–20] However, the subsequent effects in the properties of materials that are important in a wide variety of applications, from the nuclear industry to the microelectronics industry, remain a significant challenge to this day. Recently, increased computational capabilities have enabled significant progress toward a basic understanding of this question: For example, their diffusion behavior has been studied through molecular-dynamics[21–24] simulations, a technique that has also been used to find their production through a depinning mechanism in fcc copper[25] to study their role in the response of tungsten to nanoindentation[26] and in the dynamics of the bypassing of impenetrable precipitates.[27] Nonequilibrium molecular-dynamics simulations[28] suggest that shock-induced void collapse in copper occurs by the emission of shear loops rather than PMDL. Increased transmission electron microscopy performance has made possible the study of nanometer sized PMDL in BCC iron[29] and in gold,[30] and their observation in 4H-SiC when implanted with P.[31] *In situ* nanoindentation measurements of aluminum films have identified the formation of PMDL in real time.[32] The dissolution of a dislocation loop layer under the influence of inert

a)Electronic mail: agnes.maurel@espci.fr.

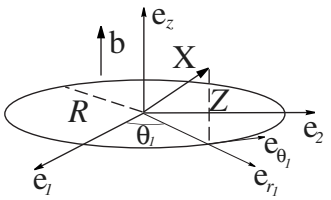

FIG. 1. Configuration of the PMDL. R denotes the radius of the loop at equilibrium, $\mathbf{X}$ is the current position, and Z is the displacement in the $\mathbf{e}_z$ direction. The Burgers vector is in the $\mathbf{e}_z$ direction.

SiO_2/Si and nitrogen-rich SiO_2/Si interfaces has been studied[33] as well as the size distribution and annealing behavior of end-of-range dislocation loops in silicon-implanted silicon.[34] The elastic stress relaxation via the formation of PMDL in a vicinity of the As–Sb nanoclusters built in a GaAs matrix has also been studied.[35] A recent calculation in the framework of anisotropic elasticity[36] has shed light on their behavior in bcc iron at high temperatures. It is appropriate then to assess in some detail what their interaction with elastic waves would be like.

In this paper, we compute the scattering cross section for an elastic wave by a PMDL following the formalism of Maurel *et al.*[5] (hereafter I).

II. BACKGROUND AND NOTATION

We consider an infinite isotropic homogeneous three dimensional continuum linear elastic medium of density ρ and elastic constants $c_{ijkl}=\lambda\delta_{ij}\delta_{kl}+\mu(\delta_{ik}\delta_{jl}+\delta_{il}\delta_{jk})$. Waves can propagate in such a medium with two characteristic velocities: longitudinal (acoustic) waves with $c_L\equiv\sqrt{(\lambda+2\mu)/\rho}$ and transverse (shear) waves with $c_T\equiv\sqrt{\mu/\rho}$. We shall denote their ratio by $\gamma=c_L/c_T$. The state of the system is characterized by (small) displacements $\mathbf{u}(\mathbf{x},t)$ of points whose equilibrium position is $\mathbf{x}$ at time t. The stress tensor σ is given in terms of the displacement vector $\mathbf{u}$ by $\sigma_{ij}=c_{ijkl}\partial u_k/\partial x_l$.

A circular, prismatic, dislocation loop (Fig. 1) of radius R and axis $\mathbf{e}_z$ at equilibrium will be considered. The dislocation position is denoted as $\mathbf{X}(s,t)$, and it is locally oriented with a unit vector $\boldsymbol{\tau}\equiv\mathbf{X}'/|\mathbf{X}'|$, where the prime denotes the derivative with respect to the Lagrangian parameter s. Time derivatives will be denoted by an overdot. The Burgers vector for the edge dislocation line is $\mathbf{b}=b\mathbf{t}$, and a glide motion is considered. For a small displacement of the dislocation line with respect to R, we will consider at dominant order $\boldsymbol{\tau}\simeq\mathbf{e}_{\theta_1}$, with $\mathbf{e}_{\theta_1}$ the orthoradial unit vector, and $\mathbf{t}=\mathbf{e}_z$. Thus, the glide motion is restricted to the displacement Z along the $\mathbf{e}_z$-axis parallel to the Burgers vector. As a function of time then, the loop is described by

$$\mathbf{X}(\theta_1,t)=R\mathbf{e}_{r_1}+Z(\theta_1,t)\mathbf{e}_z, \tag{2.1}$$

where θ_1 is the polar angle and $\mathbf{e}_{r_1}$ is the radial unit vector in the plane of the circle.

A. Response of a dislocation loop to external loading

The response of an edge dislocation to external loading is described by the equation[37]

$$\frac{\partial}{\partial t}\left(\frac{\partial\mathcal{L}}{\partial\dot{X}_k}\right)+\frac{\partial}{\partial s}\left(\frac{\partial\mathcal{L}}{\partial X_k'}\right)=\epsilon_{kjm}X_m'b_i(\sigma_{ij}+\rho\dot{X}_j\dot{u}_i)-B\dot{X}_k, \tag{2.2}$$

with

$$\mathcal{L}=|\mathbf{X}'|\left(\frac{m\dot{\mathbf{X}}^2}{2}-\Gamma\right), \tag{2.3}$$

where ϵ_{kjm} is the completely antisymmetric tensor. The first term on the right hand side of Eq. (2.2) is the usual Peach–Koehler force. The second term can be neglected when the dislocation velocities are small compared with the speed of sound, and the third term is a phenomenological drag. The mass per unit length m and the line tension Γ are given by

$$m\equiv\frac{\rho b^2}{4\pi}\ln\left(\frac{R}{\epsilon}\right)\left(1+\frac{1}{\gamma^4}\right), \tag{2.4}$$

$$\Gamma\equiv\frac{\mu b^2}{2\pi}\ln\left(\frac{R}{\epsilon}\right)\left(1-\frac{1}{\gamma^2}\right), \tag{2.5}$$

where ϵ is the short cutoff length.

We shall make the following assumptions: (i) subsonic glide (thus we neglect the velocity dependent force in Eq. (2.2)), (ii) low accelerations in order to neglect the back-reaction of radiation on the dislocation, and (iii) small amplitudes for the external stress, so that the model is linear and the possible generation of dislocations under the Frank–Read mechanism is not considered.

The equation of motion for the displacement $Z(\theta_1,t)$ is easily found from Eqs. (2.3) and (2.2) to be

$$-\frac{\Gamma}{R^2}\frac{\partial^2 Z(\theta_1,t)}{\partial\theta_1^2}+m\ddot{Z}(\theta_1,t)+B\dot{Z}(\theta_1,t)=\mu b\mathbf{M}_{lk}(\theta_1)\partial_l u_k(\mathbf{X},t), \tag{2.6}$$

where $\mathbf{M}_{lk}(\theta_1)\equiv t_l n_k+t_k n_l$, with $\mathbf{n}\equiv\boldsymbol{\tau}\times\mathbf{t}\simeq\mathbf{e}_{r1}$ (the last equality comes from the assumption of a low amplitude of the dislocation motion). If we assume in addition that the dislocation displacement has a low amplitude of motion compared to the wavelength, the Peach–Koehler force can be evaluated at the equilibrium position of the loop: $u_k(\mathbf{X},t)\simeq u_k(\mathbf{X}_0,t)$ and Eq. (2.6) becomes, in the frequency (ω) domain,

$$\frac{\partial^2 Z(\theta_1,\omega)}{\partial\theta_1^2}+\frac{R^2}{\Gamma}(m\omega^2+i\omega B)Z(\theta_1,\omega)=-\mu b\frac{R^2}{\Gamma}\mathbf{M}_{lk}(\theta_1)\partial_l u_k(\mathbf{X}_0,\omega). \tag{2.7}$$

This equation can be solved with Fourier analysis, and in the long wavelength limit, we get

$$\dot{Z}(\theta_1,\omega)=-\frac{\mu b}{m}\frac{S(\omega)}{\omega^2}\mathbf{M}_{lk}(\theta_1)\partial_l v_k(\mathbf{X}_0,\omega), \tag{2.8}$$

where $v_k\equiv\partial u_k/\partial t$ is the particle velocity, and with

$$S(\omega) \equiv \frac{\omega^2}{(\omega^2 - \omega_1^2 + i\omega B/m)} \tag{2.9}$$

and

$$\omega_1 = \sqrt{\frac{\Gamma}{mR^2}}. \tag{2.10}$$

At ultrasonic wavelengths, the denominator of $S(\omega)$ in Eq. (2.9) will be dominated by ω_1^2. Equation (2.8) thus leads to a loop response of amplitude,

$$X \approx \frac{R^2}{\lambda b} u,$$

at wavelength λ. Taking $R \sim 100$ nm, $\lambda \sim 1$ cm (as in a typical ultrasound experiment[15]), and $b \sim 1$ nm, we get

$$X \sim 10^{-3} u.$$

If we take an ultrasonic wave with an associated particle displacement of 100 nm (as would correspond, for example, to a strain of 10^{-5}), this will give a dislocation amplitude of motion of 0.1 nm. At these very small loop displacements, we ignore the corrections that would appear due to the different response different portions of the loop would have because of their different glide planes.

B. Generation of elastic waves by a dislocation loop undergoing prescribed motion

The particle velocity $\mathbf{v} \equiv \partial \mathbf{u}/\partial t$ generated by a dislocation undergoing arbitrary motion $\mathbf{X}(s,t)$ is given by Mura's integral representation,[38]

$$v_m(\mathbf{x},t) = \epsilon_{jnh} c_{ijkl} \int \int dt' ds b_i \dot{X}_n(\theta_1, t') \tau_h \times \frac{\partial}{\partial x_l} G^0_{km}(\mathbf{x} - \mathbf{X}_0, t - t'), \tag{2.11}$$

where the Green tensor G^0 is the solution of

$$\rho \frac{\partial^2}{\partial t^2} G^0_{im}(\mathbf{x},t) - c_{ijkl} \frac{\partial^2}{\partial x_j \partial x_l} G^0_{km}(\mathbf{x},t) = \delta(\mathbf{x})\delta(t)\delta_{im}, \tag{2.12}$$

with appropriate boundary conditions.

In Eq. (2.11), $\mathbf{X}_0$ has been used instead of $\mathbf{X}$ as an approximation valid for low amplitude motion. In the frequency domain, this equation becomes

$$v_m(\mathbf{x},\omega) = \epsilon_{jnh} c_{ijkl} \int ds b_i \dot{Z}(\theta_1,\omega) t_n \tau_h \frac{\partial}{\partial x_l} G^0_{km}(\mathbf{x},\omega), \tag{2.13}$$

and far from the loop, the scattered wave is obtained with the help of the asymptotic form of the Green tensor,

$$G^0_{ij}(\mathbf{x},\omega) \simeq \frac{1}{4\pi\rho} \left(\frac{\mathbf{P}_{\hat{\mathbf{x}}ij}}{c_L^2} \frac{e^{ik_L x}}{x} + \frac{(\mathbf{I} - \mathbf{P}_{\hat{\mathbf{x}}})_{ij}}{c_T^2} \frac{e^{ik_T x}}{x} \right), \tag{2.14}$$

where $k_L \equiv \omega/c_L$ and $k_T \equiv \omega/c_T$. $\mathbf{P}_{\hat{\mathbf{x}}} \equiv \hat{\mathbf{x}}\hat{\mathbf{x}}^t$ and $(\mathbf{I} - \mathbf{P}_{\hat{\mathbf{x}}})$ (with $\mathbf{I}$ as the identity matrix) are the projectors along the directions $\hat{\mathbf{x}} \equiv \mathbf{x}/x$ and perpendicularly to that direction. After some algebra, we get

$$v_m(\mathbf{x},\omega) = -\frac{i\mu b \omega R}{4\pi\rho} \int d\theta_1 \mathbf{M}_{lk}(\theta_1) \dot{Z}(\theta_1,\omega) \times \frac{x_l}{x^2} \left(\frac{\mathbf{P}_{\hat{\mathbf{x}}km}}{c_L^3} e^{ik_L x} + \frac{(\mathbf{I} - \mathbf{P}_{\hat{\mathbf{x}}})_{km}}{c_T^3} e^{ik_T x} \right). \tag{2.15}$$

III. SCATTERED ELASTIC FIELD PRODUCED BY A PMDL

The wave $\mathbf{v}^{\text{scatt}}(\mathbf{x},\omega)$, which is the scattering of an incident wave $\mathbf{v}^{\text{inc}}$ by the dislocation loop $\mathbf{X}$, is obtained in the first Born approximation by replacing the velocity $\dot{Z}$ of Eq. (2.8) in Eq. (2.15),

$$\mathbf{v}^{\text{scatt}}(\mathbf{x},\omega) = \frac{i}{4\pi} \frac{\rho b^2}{m} R c_T^4 \frac{S(\omega)}{\omega} \int d\theta_1 \mathbf{M}_{np}(\theta_1) \partial_n v_p^{\text{inc}}(\mathbf{X}_0,\omega) \times \frac{\hat{\mathbf{x}}^t}{x} \mathbf{M}(\theta_1) \left(\frac{\mathbf{P}_{\hat{\mathbf{x}}}}{c_L^3} e^{ik_L x} + \frac{(\mathbf{I} - \mathbf{P}_{\hat{\mathbf{x}}})}{c_T^3} e^{ik_T x} \right). \tag{3.1}$$

As the incident wave, we take a plane wave propagating in the direction $\hat{\mathbf{k}}_0$,

$$\mathbf{v}^{\text{inc}}(\mathbf{x},\omega) = A_L e^{i\mathbf{k}_L \mathbf{x}} \hat{\mathbf{k}}_0 + A_T e^{i\mathbf{k}_T \mathbf{x}} \hat{\mathbf{y}}_0, \tag{3.2}$$

where the index L (T) refers to longitudinal (transverse).

Substituting Eq. (3.2) in the right hand side of Eq. (3.1), we identify the longitudinal polarization with the component obtained by the projector $\mathbf{P}_{\hat{\mathbf{x}}}$ and the transversal polarization with the component in the perpendicular plane obtained by $\mathbf{I} - \mathbf{P}_{\hat{\mathbf{x}}}$. This allows us to decompose the scattered wave into a longitudinal part and a transverse part,

$$\mathbf{v}_L^{\text{scatt}}(\mathbf{x},\omega) = [f_{LL}(\hat{\mathbf{x}}) A_L + f_{LT}(\hat{\mathbf{x}}) A_T] \frac{e^{ik_L x}}{x} \hat{\mathbf{x}}, \tag{3.3}$$

$$\mathbf{v}_T^{\text{scatt}}(\mathbf{x},\omega) = [f_{TL}(\hat{\mathbf{x}}) A_L \hat{\mathbf{y}}_L + f_{TT}(\hat{\mathbf{x}}) A_T \hat{\mathbf{y}}_T] \frac{e^{ik_T x}}{x}, \tag{3.4}$$

with

$$f_{LL}(\hat{\mathbf{x}}) = -\frac{1}{4\pi} \frac{\rho b^2}{m} R c_T^4 \frac{S(\omega)}{c_L^4} \int d\theta_1 f_L(\hat{\mathbf{k}}_0, \theta_1) g_L(\hat{\mathbf{x}}, \theta_1), \tag{3.5}$$

$$f_{LT}(\hat{\mathbf{x}}) = -\frac{1}{4\pi} \frac{\rho b^2}{m} R c_T^4 \frac{S(\omega)}{c_L^3 c_T} \int d\theta_1 f_T(\hat{\mathbf{k}}_0, \theta_1) g_L(\hat{\mathbf{x}}, \theta_1), \tag{3.6}$$

$$f_{TL}(\hat{\mathbf{x}}) \hat{\mathbf{y}}_L = -\frac{1}{4\pi} \frac{\rho b^2}{m} R c_T^4 \frac{S(\omega)}{c_T^3 c_L} \int d\theta_1 f_L(\hat{\mathbf{k}}_0, \theta_1) \mathbf{g}_{\mathbf{T}}(\hat{\mathbf{x}}, \theta_1), \tag{3.7}$$

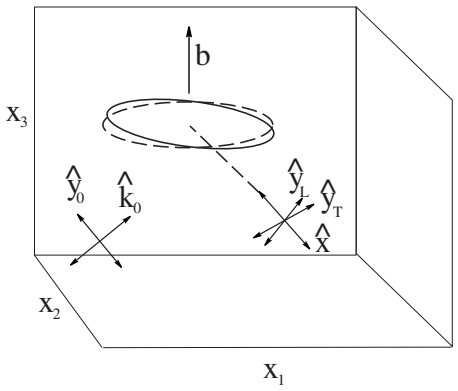

FIG. 2. Configuration for the PMDL. The dotted circle indicates the position of the dislocation loop at equilibrium, and the solid circle is the position of the loop under perturbation. The incident wave with $\hat{\mathbf{k}}_0$ wave number has a transverse polarization along the $\hat{\mathbf{y}}_0$ direction. The scattered wave in the $\hat{\mathbf{x}}$ direction (measured from the center of the loop) has transverse polarization along $\hat{\mathbf{y}}_L$ due to mode conversion and along $\hat{\mathbf{y}}_T$ due to the incident transverse wave.

$$f_{TT}(\hat{\mathbf{x}})\hat{\mathbf{y}}_T = -\frac{1}{4\pi}\frac{\rho b^2}{m}Rc_T^4\frac{S(\omega)}{c_T^4}\int d\theta_1 f_T(\hat{\mathbf{k}}_0,\theta_1)\mathbf{g_T}(\hat{\mathbf{x}},\theta_1), \tag{3.8}$$

where f_{LT}, say, is the scattering amplitude for an incident wave with polarization T to be scattered with polarization L. These amplitudes are given by $f_L(\hat{\mathbf{k}}_0,\theta_1)=\hat{\mathbf{k}}_0^t\mathbf{M}(\theta_1)\hat{\mathbf{k}}_0$, $f_T(\hat{\mathbf{k}}_0,\theta_1)=\hat{\mathbf{k}}_0^t\mathbf{M}(\theta_1)\hat{\mathbf{y}}_0$, $g_L(\hat{\mathbf{x}},\theta_1)=\hat{\mathbf{x}}^t\mathbf{M}(\theta_1)\hat{\mathbf{x}}$, and $\mathbf{g_T}(\hat{\mathbf{x}},\theta_1)=(\mathbf{I}-\hat{\mathbf{x}}\hat{\mathbf{x}}^t)\mathbf{M}(\theta_1)\hat{\mathbf{x}}$. Note that the last one is a vector and the first three are scalar functions. At this point, we make the observation that if A_L and A_T have a phase difference, then the transverse polarization will be, in general, elliptic. We come back to this point in the discussion and comparison of this problem with the pinned dislocation segment.

To have explicit expressions for the scattering amplitudes and polarization directions, we make the following choice of coordinates, illustrated in Figs. 2 and 3: We take the Burgers vector along $\mathbf{e}_z$; then, the normal vector of the dislocation loop is denoted as $\mathbf{n}=(\cos\theta_1,\sin\theta_1,0)$. Given this reference frame $(\mathbf{e}_1,\mathbf{e}_2,\mathbf{e}_z)$, the directions of the longitudinal and transverse polarizations of the incident wave are obtained by the rotation matrix $\mathbf{R}_0$ associated to the Euler angles $(\theta_0,\varphi_0,\xi_0)$: $\hat{\mathbf{k}}_0=\mathbf{R}_0\mathbf{e}_1$ and $\hat{\mathbf{k}}_0=\mathbf{R}_0\mathbf{e}_2$ (see Appendix A).

The scattered wave propagates radially in the direction $\hat{\mathbf{x}}$, and we used the Euler angles (θ,φ,ξ) to characterize its

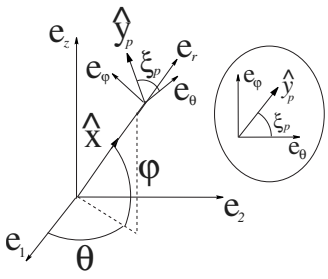

FIG. 3. Definition of the Euler angles (θ,φ,ξ_p) characterizing the scattered wave. The index p stands for either L and T (the scattered transverse waves produced by either the longitudinal or the transverse incident waves). We have the same definition to characterize the incident wave with $(\theta_0,\varphi_0,\xi_0)$.

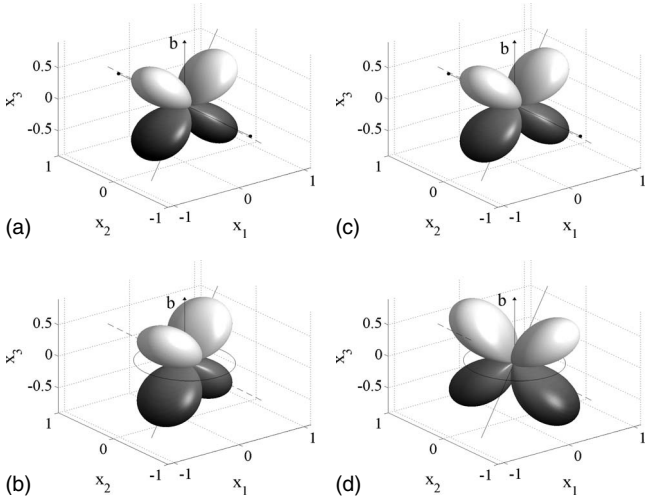

FIG. 4. Angular dependence of the scattering functions f_{LL} (top) and f_{LT} (bottom). The left-hand-side panels illustrate the behavior for the case of a dislocation segment along the x_2-axis, indicated here as a solid line with markers at the end points. The right-hand-side panels illustrate the behavior for the case of a prismatic loop lying along the (x_1,x_2)-plane, indicated here by a solid line circle. The incident wave is characterized by $\varphi_0=\pi/4$, $\theta_0=\pi/8$, and $\xi_0=\pi/3$. Its direction of propagation is indicated by a solid line, and the direction of polarization of the transverse incident wave is indicated by a dotted line. The Burgers vector is along the x_3-axis in all cases.

direction of propagation $\hat{\mathbf{x}}=\mathbf{R}\mathbf{e}_1$ and the direction of polarization of the transverse component through $\hat{\mathbf{y}}_L$ and $\hat{\mathbf{y}}_T$.

With the chosen reference frame, the vector and matrix product that defines the auxiliary functions $f_L(\hat{\mathbf{k}}_0,\theta_1)$, $f_T(\hat{\mathbf{k}}_0,\theta_1)$ and $g_L(\hat{\mathbf{x}},\theta_1)$, $\mathbf{g}_T(\mathbf{x},\theta_1)$ can be computed, and the integration over $\theta_1\in[0,2\pi]$ that appears in the scattering amplitudes is performed. The intermediate steps of this computation are collected in Appendix A. Our final expression for scattered amplitudes is

$$f_{LL}(\hat{\mathbf{x}}) = -\frac{1}{4}\frac{\rho b^2}{m}R\frac{S(\omega)}{\gamma^4}\sin 2\varphi\,\sin 2\varphi_0\cos(\theta-\theta_0), \tag{3.9}$$

$$f_{LT}(\hat{\mathbf{x}}) = -\frac{1}{4}\frac{\rho b^2}{m}R\frac{S(\omega)}{\gamma^3}\{\sin 2\varphi[\sin\varphi_0\cos\xi_0\sin(\theta-\theta_0) + \sin\xi_0\cos 2\varphi_0\cos(\theta-\theta_0)]\}, \tag{3.10}$$

$$f_{TL}(\hat{\mathbf{x}})\hat{\mathbf{y}}_L = -\frac{1}{4}\frac{\rho b^2}{m}R\frac{S(\omega)}{\gamma}\sin 2\varphi_0[\sin\varphi\sin(\theta-\theta_0)\mathbf{e}_\theta + \cos 2\varphi\cos(\theta-\theta_0)\mathbf{e}_\varphi], \tag{3.11}$$

$$f_{TT}(\hat{\mathbf{x}})\hat{\mathbf{y}}_T = -\frac{1}{4}\frac{\rho b^2}{m}RS(\omega)\{\sin\varphi[\sin\varphi_0\cos\xi_0\cos(\theta-\theta_0) - \cos 2\varphi_0\sin\xi_0\sin(\theta-\theta_0)]\mathbf{e}_\theta + \cos 2\varphi[\sin\varphi_0\cos\xi_0\sin(\theta-\theta_0) + \cos 2\varphi_0\sin\xi_0\cos(\theta-\theta_0)]\mathbf{e}_\varphi\}. \tag{3.12}$$

As expected, the problem is invariant by rotation around $\mathbf{e}_z$ (invariance by the transformation $\theta\to\theta+\theta'$ and $\theta_0\to\theta_0+\theta'$).

Figure 4 shows the typical behavior of the scattering functions f_{LL} and f_{LT} as a function of the angle. The case of

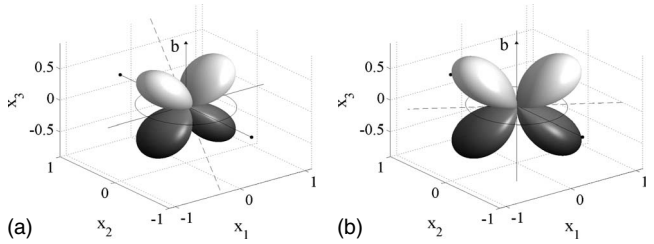

FIG. 5. Typical displacement of the loop and corresponding motions of the two segments forming a dipole. The two arrangements produce the same scattering patterns independent of d [the same strength is obtained for $L=\pi R(\pi/4)^{2/3}$].

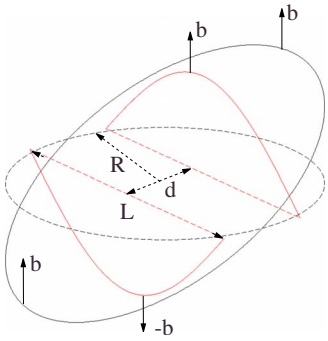

FIG. 6. (Color online) Angular dependence of the scattering function f_{LT}. Left-hand-side panel: The incident wave propagates in the plane of the loop along the x_1 direction, indicated by a solid line; the direction of polarization of the incident transverse wave is indicated by a dotted line. The same scattering pattern is produced by a dislocation segment in the same plane oriented perpendicularly to the direction of propagation of the incident wave, indicated by a solid line with markers at the end points. Right-hand-side panel: The incident wave propagates along the Burgers vector (x_3-direction), indicated by a solid line; the direction of polarization of the incident transverse wave is indicated by a dotted line. The same scattering pattern is produced by a dislocation segment in the plane of the loop oriented perpendicularly to the direction of polarization of the incident transverse wave, indicated by a solid line with markers at the end points.

the pinned segment is presented as well for comparison (from Ref. 4, see also Appendix B). Qualitatively, the symmetry of the scattering functions for the pinned dislocation segment is determined by the directions of the dislocation line and the direction of the Burgers vector only (labeled x_2 and x_3 in Fig. 5), while the symmetry of the scattering functions for the prismatic loop depends on the direction of the incident wave. A more detailed comparison between the two configurations is presented in the forthcoming section.

A. Discussion

We have calculated the response of a dislocation loop under the effect of an incident wave [Eq. (2.8)] as well as the subsequent scattered wave [Eqs. (3.9)–(3.12)] in the long wavelength limit. As previously said, a similar calculation has been performed for a pinned dislocation segment,[4] and the question arises on what the similarities and differences are. The answer to this question depends on the quantity we look at. For an individual dislocation loop, certain similarities with a dislocation segment (in terms of the scattering process) can be pointed out, but there are also significant differences that could be used to discriminate between the two dislocation geometries. On the other hand, the collective behavior of an ensemble of prismatic loops (in terms of the multiple scattering process) resembles those for an ensemble of pinned dislocation segments. For ease of comparison, we give in Appendix B the expressions of the dislocation motion and the expression of the scattering functions in the case of the pinned dislocation segment using the conventions of Fig. 2 (namely, with **b** along the $\mathbf{e}_z$-axis).

1. Equivalence of a loop with a dipole

There are two simple cases when a loop behaves as two pinned segments with opposite Burgers vectors (or dipole).

(1) The incident wave propagates perpendicularly to the Burgers vector **b** in the plane of the dislocation loop, say, in the x_1-direction ($\varphi_0=\theta_0=0$). Then, the loop reacts to this incident wave as two dislocation segments (a dipole) both oriented perpendicularly to the direction of the incident wave (x_2-direction) and having opposite Burgers vector. Indeed, we have in that case: for the loop

$$\dot{Z} \propto A_T b(\pi R)^2 \sin\xi_0 \cos\theta_1 \sin\omega t, \tag{3.13}$$

which means that the loop oscillates with two fixed points along the x_2-axis, namely, $x_2=\pm R$ (see Fig. 6). Incidentally, note that the longitudinal wave does not interact with the loop in this geometry. The motion of a dislocation segment oriented along x_2 is given by (see I):

$$\dot{Z}_s \propto A_T b L^2 \sin\xi_0 \cos\theta_0 \cos(\pi x_2/L)\sin\omega t, \tag{3.14}$$

and the similarity is clear.

The above expressions for $\dot{Z}$ are given in the limit $\omega \to 0$ (thus, $\omega \ll \omega_1$). Of course, this similarity in the dislocation motions (the loop and the dislocation dipole) is recovered in the scattering wave. In both cases, we get $f_{LL}=f_{TL}=0$ and

$$f_{LT} \propto Cb^2 \sin\xi_0 \sin 2\varphi \cos\theta,$$

$$f_{TT}\hat{\mathbf{y}} \propto Cb^2 \sin\xi_0(-\sin\varphi \sin\theta \mathbf{e}_\theta + \cos 2\varphi \cos\theta \mathbf{e}_\varphi), \tag{3.15}$$

with C as a constant, $C=(\pi R)^3$ for the loop, and $C=(4/\pi)^2 L^3$ for the dipole.

(2) The incident wave propagates along the Burgers vector ($\varphi_0=\pi/2$). In that case, the motion of the dislocation loop is

$$\dot{Z} \propto A_T b(\pi R)^2 \sin(\theta_1-\theta_0)\cos\omega t, \tag{3.16}$$

where θ_0 denotes the direction of polarization of the transverse incident wave in the plane of the loop (again, in this case, the longitudinal wave does not interact with the dislocation). A similar motion is mimicked by a dipole of dislocation segments oriented perpendicularly to the transverse incident wave. Without loss of generality,

we can consider the incident transverse polarization along x_2 ($\theta_0=\pi/2$), and we get

$$\dot{Z} \propto A_T b(\pi R)^2 \cos\theta_1 \cos\omega t. \tag{3.17}$$

The response of one dislocation segment to the same wave is

$$\dot{Z}_s \propto A_T b L^2 \cos\pi s/L \cos\omega t. \tag{3.18}$$

Again, we observe in both cases an oscillatory motion with two fixed points at $x_2=\pm R, \pm L/2$. Also, the corresponding scattering functions are similar, with $f_{LL}=f_{TL}=0$ in both cases and

$$f_{LT} \propto Cb^2 \sin 2\varphi \cos\theta,$$

$$f_{TT}\hat{\mathbf{y}} \propto Cb^2(-\sin\varphi \sin\theta \mathbf{e}_\theta + \cos 2\varphi \cos\theta \mathbf{e}_\varphi) \tag{3.19}$$

(with the same convention for C as in the previous case).

2. Elliptic polarization of the transverse wave

An important qualitative difference between the scattering by a dislocation loop and a segment is the polarization of the transverse scattered wave. In the case of a segment,[4] a linearly transversely polarized incident wave ($A_T\hat{\mathbf{y}}_0$) will be scattered as linearly transversely polarized as well, namely, with a direction of polarization $\hat{\mathbf{p}}_s$ in the $(\mathbf{e}_\theta,\mathbf{e}_\varphi)$-plane given by (see Appendix B),

$$\hat{\mathbf{p}}_s = \begin{pmatrix} \cos\phi \\ \sin\phi \end{pmatrix} \cos\omega t, \tag{3.20}$$

with $\tan\phi=-\cos 2\varphi/(\sin\varphi\tan\theta)$.

In the case of the prismatic loop, an incident wave with a linear transverse polarization will be, in general, scattered with an elliptic transverse polarization. We denote $A_L=C\ A_T e^{i\alpha}$, with C real. Incidentally, this corresponds to an incident wave that is, in general, elliptically polarized when we consider the total displacement: The transverse incident wave is linearly polarized (along $\hat{\mathbf{y}}_0$), and the total displacement is elliptically polarized in the plane $(\hat{\mathbf{k}}_0,\hat{\mathbf{y}}_0)$ (this is typically the case of Rayleigh waves). However, in this paper, we focus on the polarization of the transverse wave only. From Eqs. (3.4), (3.11), and (3.12), the direction of polarization of the transverse scattered wave in the $(\mathbf{e}_\theta,\mathbf{e}_\varphi)$-plane is given by

$$\hat{\mathbf{p}} = \begin{pmatrix} \cos\phi & \sin\phi \\ -\sin\phi & \cos\phi \end{pmatrix} \begin{pmatrix} \cos\omega t \\ r\sin\omega t \end{pmatrix}, \tag{3.21}$$

which means that the resulting transverse wave is elliptically polarized. Here, r is the aspect ratio of the ellipse, and ϕ is its inclination as in Fig. 7 (we can use as well the Jones polarization vector[39]). In general, the expressions for r and ϕ are quite intricate. Let us consider the particular case where the scattered wave is measured in the forward direction only. Then, the orientation of the incident wave $\hat{\mathbf{k}}_0$ and, thus, of the measured scattered wave $\hat{\mathbf{x}}$ is varied. The whole problem depends now on $\varphi=\varphi_0$ only (the invariance by rotation around $\mathbf{e}_z$ makes the problem independent on $\theta=\theta_0$) and depends on ξ_0, the direction of polarization of the incident transverse wave. We find in this case

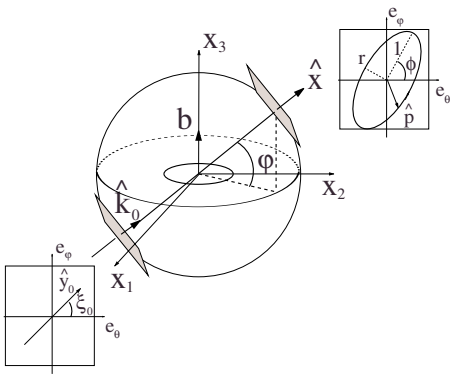

FIG. 7. (Color online) We consider the polarization of the transverse scattered wave in the $(\mathbf{e}_\theta,\mathbf{e}_\varphi)$-plane. The particular case of the forward scattering is considered: $\hat{\mathbf{x}}=\hat{\mathbf{k}}_0$. In the $(\mathbf{e}_\theta,\mathbf{e}_\varphi)$-plane, the linear polarization of the transverse incident wave is characterized by ξ_0, and the elliptical polarization of the transverse scattered wave $\hat{\mathbf{p}}_s$ is characterized by the parameters ϕ and r.

$$\hat{\mathbf{p}} = \begin{pmatrix} \sin\varphi\cos\xi_0\cos\omega t \\ C/\gamma\cos 2\varphi\sin 2\varphi\cos(\omega t+\alpha)+\cos^2 2\varphi\sin\xi_0\cos\omega t \end{pmatrix}, \tag{3.22}$$

from which r and ϕ can be deduced. Results are shown in Fig. 8 for $\xi_0=\pi/2$ ($C/\gamma=1$) as a function of the direction of incident wave φ for various α-values (this latter value depends on the experimental conditions). As expected, the polarization of the scattered transverse wave is linear for $\alpha=0,\pi$ (in that case, both longitudinal and transverse incident waves have no phase difference) while any phase difference α in the incident wave produces the elliptic polarization of the transverse scattered wave. Some fixed points are (i) $\varphi=0$, where the incident wave propagates in the plane of the loop. The transverse scattered wave is linearly polarized along $\mathbf{e}_\varphi$ independently of the polarization of the incident wave and the phase difference α. (ii) $\varphi=45°$, the same phenomenon occurs with a transverse scattered wave linearly polarized along $\mathbf{e}_\theta$. Finally, (iii) the incident wave propagates along the Burgers vector ($\varphi=90°$), in which case the transverse scattered wave is linearly polarized in the same direction as the incident transverse wave ($\phi=\xi_0$).

3. Attenuation produced by an ensemble of prismatic loops

A characteristic signature of dislocations in a material is the acoustic attenuation they produce. We will see that a significant similarity between dislocation loops and dislocation segments is that both produce a different attenuation on longitudinal and transverse waves, a fact that has been experimentally measured.[12]

In a multiple scattering theory, there may exist a coherent wave propagating with an effective wave velocity and with its amplitude attenuated due to the energy loss produced by the viscous force on the dislocations and also by the transfer of energy from the coherent to the incoherent wave that occurs due to scattering. This coherent wave propagates in an

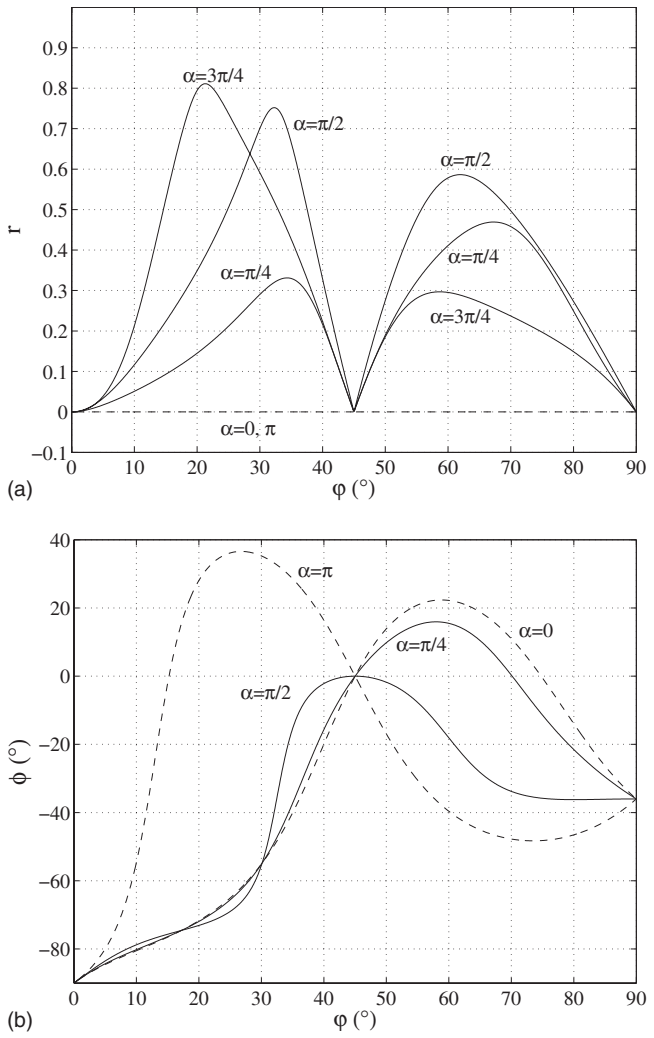

FIG. 8. Variation in the polarization of the transverse wave observed in the forward scattering as a function of φ. r and ϕ are deduced by identifying Eq. (3.21) with Eq. (3.22); here, $\xi_0=35°$ $(\pi/5)$, and we have used $C/\gamma=1$ in Eq. (3.22). In the dotted line, the case $\alpha=0,\pi$ corresponds to a resulting linear polarization of the transverse scattered wave $(r=0)$.

effective medium that corresponds to the average over all realizations of the disordered medium. The actual computation for an ensemble of loops is very similar to the case of an ensemble of segments.[5] We have found the phase velocities $v_{L,T}$ and the attenuations $\alpha_{L,T}$ for both the longitudinal and transverse waves propagating through many dislocation loops as the real and imaginary parts of the effective wave numbers. In the long wavelength limit, we get

$$v_a = c_a(1 - \mathcal{C}_a n R^3), \tag{3.23}$$

$$\alpha_a = \mathcal{C}'_a \frac{B\omega^2}{\rho b^2 c_T^3} n R^5, \tag{3.24}$$

where $a=L,T$, with $\mathcal{C}_L=8\pi^2/(15\gamma^2)$, $\mathcal{C}_T=2\pi^2/5$, $\mathcal{C}'_L=16\pi^3/(15\gamma^3)$, and $\mathcal{C}'_T=4\pi^3/5$ for the loop, to be compared with

$$v_a^s = c_a(1 - \mathcal{C}_a n L^3), \tag{3.25}$$

$$\alpha_a^s = \mathcal{C}' \frac{B\omega^2}{\rho b^2 c_T^3} n L^5, \tag{3.26}$$

with $\mathcal{C}_L=32/(15\pi^3\gamma^2)$, $\mathcal{C}_T=8/5\pi^3$, $\mathcal{C}'_L=64/(15\pi^4\gamma^3)$, and $\mathcal{C}'_T=16/(5\pi^4)$ for the dislocation segment (see Eqs. (6.4) and (6.5) in Ref. 5).

It follows that loops and segments of similar lengths produce similar changes in the velocities and similar attenuations. A more significant similarity is the difference in the attenuations predicted for longitudinal and transverse waves. This difference is experimentally measured by measuring the quality factor in RUS or electromagntic acoustic resonance experiments (Ref. 12; see also Ref. 5), $Q_a^{-1} \propto \alpha_a c_a^2$. In both cases, loops and segments, we have

$$\frac{Q_T^{-1}}{Q_L^{-1}} = \frac{3}{4\gamma} \sim 1.3 - 1.56, \tag{3.27}$$

where the numerical values are obtained using the typical values of γ in most materials. This ratio is exactly the same compared to the one obtained for an ensemble of dislocation segments and is in very good agreement with experimental measurements.

Resonant ultrasound spectroscopy measurements[15] are sensitive to shifts in the shear wave velocity of about 1%. Assuming a typical dislocation loop radius of about 100 nm, this would indicate a loop density of 10^{18} m^{-3} as the current threshold for detection through ultrasonic techniques.

IV. CONCLUDING REMARKS

We have studied the behavior of elastic waves interacting with a prismatic loop in the long wavelength limit. This interaction is as follows: the incident elastic waves induce an oscillation of the dislocation loop, and this motion produces outgoing (scattered) waves. The corresponding scattering functions have been calculated. Mode conversions are possible between longitudinal and transverse waves, one possible consequence of which is to change the polarization of an incident transverse wave from linear to elliptical.

As we saw in Eqs. (3.13)–(3.16), the response of a PMDL $X(\theta_1,t)$ has two nodal fixed points, and therefore it is natural to compare the results of the pinned dislocation dipole with the dislocation loop of similar size. For some directions of incidence, the scattering patterns coincide.

One can also ask about the properties of a coherent wave propagating through an elastic medium filled with randomly placed, and oriented, PMDLs, a question that was studied in detail in Ref. 5 for straight segments. While the *individual* scattering properties of a dislocation segment are quite different from those of the dislocation loop, we have shown that, in a long wavelength limit, averaged quantities such as effective velocities and attenuation coefficients are roughly independent of the characteristic geometry of the dislocation.

ACKNOWLEDGMENTS

The authors acknowledge support from the Scientific Computing Advanced Training (SCAT) project through EuropeAid Contract No. II-0537-FC-FA (http://www.scat-alfa.eu). We are grateful to ECOS-CONICYT as well as to

Fondap Grant No. 11980002. F.B. also acknowledges the financial support from Fondecyt Grant No. 1060820 and Anillo ACT 15. Useful discussions with A. Sepúlveda are gratefully acknowledged. Our interest in dislocation loops was enhanced by discussions with M. Barsoum.

APPENDIX A: TECHNICAL CALCULATIONS ON THE SCATTERING FUNCTIONS

This appendix provides the details needed to obtain Eqs. (3.9)–(3.12). The Burgers vector is defined as $\mathbf{b}=b\mathbf{e}_3$; the vector normal to the dislocation line is denoted as $\mathbf{n}=\tilde{\mathbf{R}}\mathbf{e}_1$, with

$$\tilde{\mathbf{R}}=\begin{pmatrix}\cos\theta_1 & -\sin\theta_1 & 0\\ \sin\theta_1 & \cos\theta_1 & 0\\ 0 & 0 & 1\end{pmatrix}. \tag{A1}$$

With this definition, the matrix $\mathbf{M}$ defined by $\mathbf{M}_{lk}\equiv t_l n_k + t_k n_l$ takes the form $\mathbf{M}=\tilde{\mathbf{R}}\mathbf{e}_1\mathbf{e}_3^t+\mathbf{e}_3\mathbf{e}_1^t\tilde{\mathbf{R}}^t$.

The longitudinal and transverse polarizations of the incident wave were chosen, respectively, as $A_L\mathbf{R}_0\mathbf{e}_1$ and $A_T\mathbf{R}_0\mathbf{e}_2$, with $\mathbf{R}_0$ as the rotation matrix of Euler angles $(\theta_0,\varphi_0,\xi_0)$ given by

$$\mathbf{R}_0=\begin{pmatrix}\cos\varphi_0\cos\theta_0 & -\sin\theta_0\cos\xi_0-\sin\varphi_0\cos\theta_0\sin\xi_0 & -\sin\theta_0\sin\xi_0-\sin\varphi_0\cos\theta_0\cos\xi_0\\ \cos\varphi_0\sin\theta_0 & \cos\theta_0\cos\xi_0-\sin\varphi_0\sin\theta_0\sin\xi_0 & -\cos\theta_0\sin\xi_0-\sin\varphi_0\sin\theta_0\cos\xi_0\\ \sin\varphi_0 & \cos\varphi_0\sin\xi_0 & \cos\varphi_0\cos\xi_0\end{pmatrix}. \tag{A2}$$

Now, we compute the functions that appear inside the integrals in Eqs. (3.5)–(3.8). The direction of propagation of the incident wave $\hat{\mathbf{k}}_0=\mathbf{R}_0\mathbf{e}_1$ is given by the first column of $\mathbf{R}_0$ and therefore an explicit expression for $f_L(\hat{\mathbf{k}}_0,\theta_1)=\hat{\mathbf{k}}_0^t\mathbf{M}(\theta_1)\hat{\mathbf{k}}_0$ is

$$f_L(\hat{\mathbf{k}}_0,\theta_1)=2\mathbf{R}_{0_{31}}(\cos\theta_1\mathbf{R}_{0_{11}}+\sin\theta_1\mathbf{R}_{0_{21}}). \tag{A3}$$

Similarly, because $\hat{\mathbf{y}}_0=\mathbf{R}_0\mathbf{e}_1$, an explicit expression for $f_T(\hat{\mathbf{k}}_0,\theta_1)=\hat{\mathbf{k}}_0^t\mathbf{M}(\theta_1)\hat{\mathbf{y}}_0$ is

$$\begin{aligned}f_T(\hat{\mathbf{k}}_0,\theta_1)=&\cos\theta_1(\mathbf{R}_{0_{11}}\mathbf{R}_{0_{32}}+\mathbf{R}_{0_{12}}\mathbf{R}_{0_{31}})\\&+\sin\theta_1(\mathbf{R}_{0_{21}}\mathbf{R}_{0_{32}}+\mathbf{R}_{0_{22}}\mathbf{R}_{0_{31}}).\end{aligned} \tag{A4}$$

For $g_L(\hat{\mathbf{x}},\theta_1)=\hat{\mathbf{x}}^t\mathbf{M}(\theta_1)\hat{\mathbf{x}}$, the computation is the same for $f_L(\hat{\mathbf{k}}_0,\theta_1)$ because $\hat{\mathbf{x}}=\mathbf{R}\mathbf{e}_1$, with $\mathbf{R}$ as the rotation matrix of Euler angles (θ,φ,ξ). Thus,

$$g_L(\hat{\mathbf{x}})=2\mathbf{R}_{31}(\cos\theta_1\mathbf{R}_{11}+\sin\theta_1\mathbf{R}_{21}). \tag{A5}$$

Finally, for the vector quantity $\mathbf{g}_T(\hat{\mathbf{x}},\theta_1)$,

$$\begin{aligned}\mathbf{g}_\mathbf{T}(\hat{\mathbf{x}},\theta_1)&=[\mathbf{I}-\hat{\mathbf{x}}\hat{\mathbf{x}}^\mathbf{t}]\mathbf{M}(\theta_1)\hat{\mathbf{x}}\\&=(\mathbf{e}_\theta^\mathbf{t}[\mathbf{I}-\hat{\mathbf{x}}\hat{\mathbf{x}}^\mathbf{t}]\mathbf{M}\hat{\mathbf{x}})\mathbf{e}_\theta+(\mathbf{e}_\varphi^\mathbf{t}[\mathbf{I}-\hat{\mathbf{x}}\hat{\mathbf{x}}^\mathbf{t}]\mathbf{M}(\theta_1)\hat{\mathbf{x}})\mathbf{e}_\varphi,\end{aligned} \tag{A6}$$

where the components are

$$\mathbf{e}_\theta^t(\mathbf{I}-\hat{\mathbf{x}}\hat{\mathbf{x}}^t)\mathbf{M}\hat{\mathbf{x}}=\cos\theta_1\mathbf{e}_{\theta_1}x_3+\sin\theta_1\mathbf{e}_{\theta_2}x_3, \tag{A7}$$

$$\begin{aligned}\mathbf{e}_\varphi^t(\mathbf{I}-\hat{\mathbf{x}}\hat{\mathbf{x}}^t)\mathbf{M}\hat{\mathbf{x}}=&\cos\theta_1(\mathbf{e}_{\varphi_3}x_1+\mathbf{e}_{\varphi_1}x_3)\\&+\sin\theta_1(\mathbf{e}_{\varphi_3}x_2+\mathbf{e}_{\varphi_2}x_3).\end{aligned} \tag{A8}$$

Multiplying the previous terms as required by Eqs. (3.5)–(3.8) and doing the integrals (where only terms multiplying $\sin^2\theta_1$ or $\cos^2\theta_1$ survive), we obtain the scattering for amplitude functions

$$\begin{aligned}f_{LL}(\hat{\mathbf{x}})=&-\frac{1}{4}\frac{\rho b^2}{m}Rc_T^4\frac{S(\omega)}{c_L^4}(4\mathbf{R}_{0_{31}}\mathbf{R}_{0_{11}}\mathbf{R}_{31}\mathbf{R}_{11}\\&+4\mathbf{R}_{0_{31}}\mathbf{R}_{0_{21}}\mathbf{R}_{31}\mathbf{R}_{21}),\end{aligned} \tag{A9}$$

$$\begin{aligned}f_{LT}(\hat{\mathbf{x}})=&-\frac{1}{4}\frac{\rho b^2}{m}Rc_T^4\frac{S(\omega)}{c_L^3c_T}[(\mathbf{R}_{0_{11}}\mathbf{R}_{0_{32}}+\mathbf{R}_{0_{12}}\mathbf{R}_{0_{31}})2\mathbf{R}_{31}\mathbf{R}_{11}\\&+(\mathbf{R}_{0_{21}}\mathbf{R}_{0_{32}}+\mathbf{R}_{0_{22}}\mathbf{R}_{0_{31}})2\mathbf{R}_{31}\mathbf{R}_{21}],\end{aligned} \tag{A10}$$

$$\begin{aligned}f_{TL}(\hat{\mathbf{x}})\hat{\mathbf{y}}_L=&-\frac{1}{4}\frac{\rho b^2}{m}Rc_T^4\frac{S(\omega)}{c_T^3c_L}\{(2\mathbf{e}_{\theta_1}x_3\mathbf{R}_{0_{31}}\mathbf{R}_{0_{11}}\\&+2\mathbf{e}_{\theta_2}x_3\mathbf{R}_{0_{31}}\mathbf{R}_{0_{21}})\mathbf{e}_\theta+[2(\mathbf{e}_{\varphi_3}x_1\\&+\mathbf{e}_{\varphi_1}x_3)\mathbf{R}_{0_{31}}\mathbf{R}_{0_{11}}+2(\mathbf{e}_{\varphi_3}x_2\\&+\mathbf{e}_{\varphi_2}x_3)\mathbf{R}_{0_{31}}\mathbf{R}_{0_{21}}]\mathbf{e}_\varphi\},\end{aligned} \tag{A11}$$

$$\begin{aligned}f_{TT}(\hat{\mathbf{x}})\hat{\mathbf{y}}_T=&-\frac{1}{4}\frac{\rho b^2}{m}RS(\omega)\{[\mathbf{e}_{\theta_1}x_3(\mathbf{R}_{0_{11}}\mathbf{R}_{0_{32}}+\mathbf{R}_{0_{12}}\mathbf{R}_{0_{31}})\\&+\mathbf{e}_{\theta_2}x_3(\mathbf{R}_{0_{21}}\mathbf{R}_{0_{32}}+\mathbf{R}_{0_{22}}\mathbf{R}_{0_{31}})]\mathbf{e}_\theta+[(\mathbf{e}_{\varphi_3}x_1\\&+\mathbf{e}_{\varphi_1}x_3)(\mathbf{R}_{0_{11}}\mathbf{R}_{0_{32}}+\mathbf{R}_{0_{12}}\mathbf{R}_{0_{31}})+(\mathbf{e}_{\varphi_3}x_2+\mathbf{e}_{\varphi_2}x_3)\\&\times(\mathbf{R}_{0_{21}}\mathbf{R}_{0_{32}}+\mathbf{R}_{0_{22}}\mathbf{R}_{0_{31}})]\mathbf{e}_\varphi\}.\end{aligned} \tag{A12}$$

Now, the product of rotation matrices can be made explicit. The results are Eqs. (3.9)–(3.12).

APPENDIX B: PINNED SEGMENT

In this appendix, we provide the formulas of Ref. 4 for dislocation segments in a reference frame that facilitates a comparison with results for dislocation loops provided in this

work. In Ref. 4, the convention is as follows: The Burgers vector is oriented along the x_1 direction, and the segment is oriented along the x_3 direction. In the present case, the symmetry of the loop suggests choosing the Burgers vector along x_3 (leading to an invariance by rotation $\theta-\theta_0$). To make the comparison with the pinned segment, we give here the result on the scattering functions for the pinned segment with the same convention of **b** along x_3, and we arbitrarily choose the segment direction along x_2. The scattering functions now are

$$f_{LL}(\hat{\mathbf{x}}) = -\frac{2}{\pi^3}\frac{\rho b^2}{m}\gamma^{-4}LS(\omega)f_L(\hat{\mathbf{k}}_0)g_L(\hat{\mathbf{x}}),$$

$$f_{LT}(\hat{\mathbf{x}}) = -\frac{2}{\pi^3}\frac{\rho b^2}{m}\gamma^{-3}LS(\omega)f_T(\hat{\mathbf{k}}_0)g_L(\hat{\mathbf{x}}),$$

$$f_{TL}(\hat{\mathbf{x}}) = -\frac{2}{\pi^3}\frac{\rho b^2}{m}\gamma^{-1}LS(\omega)f_L(\hat{\mathbf{k}}_0)g_T(\hat{\mathbf{x}}),$$

$$f_{TT}(\hat{\mathbf{x}}) = -\frac{2}{\pi^3}\frac{\rho b^2}{m}LS(\omega)f_T(\hat{\mathbf{k}}_0)g_T(\hat{\mathbf{x}}), \tag{B1}$$

with

$$g_L(\hat{\mathbf{x}}) = \sin 2\varphi \cos\theta,$$

$$g_T(\hat{\mathbf{x}})\hat{\mathbf{y}} = -\sin\varphi \sin\theta \mathbf{e}_\theta + \cos 2\varphi \cos\theta \mathbf{e}_\varphi \tag{B2}$$

and

$$f_L(\hat{\mathbf{k}}_0) = \sin 2\varphi_0 \cos\theta_0,$$

$$f_T(\hat{\mathbf{k}}_0) = \cos 2\varphi_0 \cos\theta_0 \sin\xi_0 - \sin\varphi_0 \sin\theta_0 \cos\xi_0. \tag{B3}$$

It follows that the direction of polarization of the transverse wave is linear and depends only on the direction of the observation $\hat{\mathbf{x}}$: In the $(\mathbf{e}_\theta, \mathbf{e}_\varphi)$-plane, the direction of polarization of the transverse wave is

$$\hat{\mathbf{p}} = \begin{pmatrix} -\sin\varphi \sin\theta \\ \cos 2\varphi \cos\theta \end{pmatrix}, \tag{B4}$$

independently of the incident wave.

[1] A. Maurel, J.-F. Mercier, and F. Lund, J. Acoust. Soc. Am. **115**, 2773 (2004).
[2] A. Maurel, J.-F. Mercier, and F. Lund, Phys. Rev. B **70**, 024303 (2004).
[3] A. Maurel, V. Pagneux, D. Boyer, and F. Lund, Mater. Sci. Eng., A **400–401**, 222 (2005).
[4] A. Maurel, V. Pagneux, F. Barra, and F. Lund, Phys. Rev. B **72**, 174110 (2005).
[5] A. Maurel, V. Pagneux, F. Barra, and F. Lund, Phys. Rev. B **72**, 174111 (2005).
[6] A. Maurel, V. Pagneux, D. Boyer, and F. Lund, Proc. R. Soc. London, Ser. A **462**, 2607 (2006).
[7] A. Maurel, V. Pagneux, F. Barra, and F. Lund, Phys. Rev. B **75**, 224112 (2007).
[8] A. Maurel, V. Pagneux, F. Barra, and F. Lund, J. Acoust. Soc. Am. **121**, 3418 (2007).
[9] A. V. Granato and K. Lücke, J. Appl. Phys. **27**, 583 (1956).
[10] A. V. Granato and K. Lücke, J. Appl. Phys. **27**, 789 (1956).
[11] D. Shilo and E. Zolotoyabko, Phys. Rev. Lett. **91**, 115506 (2003), and references therein.
[12] H. M. Ledbetter and C. Fortunko, J. Mater. Res. **10**, 1352 (1995); H. Ogi, H. M. Ledbetter, S. Kim, and M. Hirao, J. Acoust. Soc. Am. **106**, 660 (1999); H. Ogi, N. Nakamura, M. Hirao, and H. M. Ledbetter, Ultrasonics **42**, 183 (2004).
[13] X.-G. Zhang, W. A. Simpson, Jr., and J. M. Vitek, J. Acoust. Soc. Am. **116**, 109 (2004).
[14] A. Maurel, V. Pagneux, F. Barra, and F. Lund, "Ultrasound as a probe of Plasticity? The interaction of elastic waves with dislocations," Int. J. Bifurcation Chaos Appl. Sci. Eng. (to be published).
[15] F. Barra, A. Caru, M. T. Cerda, R. Espinoza, A. Jara, F. Lund, and N. Mujica, "Measuring dislocation density in aluminum with resonant ultrasound spectroscopy," e-print arXiv:0808.1561v1.
[16] B. C. Masters, Philos. Mag. **11**, 881 (1965).
[17] B. L. Eyre and A. F. Bartlett, Philos. Mag. **12**, 261 (1965); J. Nucl. Mater. **47**, 143 (1973).
[18] T. J. Bullough, C. A. English, and B. L. Eyre, Proc. R. Soc. London, Ser. A **534**, 85 (1991).
[19] H. Kawanishi, S. Ishino, and E. Kuramoto, J. Nucl. Mater. **141–143**, 899 (1986).
[20] L. L. Horton and K. Farrell, J. Nucl. Mater. **122**, 684 (1984).
[21] N. Soneda and T. Díaz de la Rubia, Philos. Mag. A **81**, 331 (2001).
[22] Y. Osetsky, D. J. Bacon, B. N. Singh, and B. Wirth, J. Nucl. Mater. **307–311**, 852 (2002).
[23] J. Marian, B. D. Wirth, A. Caro, B. Sadigh, G. R. Odette, J. M. Perlado, and T. Diaz de la Rubia, Phys. Rev. B **65**, 144102 (2002).
[24] T. Hatano, Phys. Rev. B **77**, 064108 (2008).
[25] J. H. A. Hagelaar, E. Bitzek, C. F. J. Flipse, and P. Gumbsch, Phys. Rev. B **73**, 045425 (2006).
[26] T. Hatano, Phys. Rev. B **74**, 020102(R) (2006).
[27] L. P. Davila, P. Erhart, E. M. Bringa, M. A. Meyers, V. A. Lubarda, M. S. Schneider, R. Becker, and M. Kumar, Appl. Phys. Lett. **86**, 161902 (2005).
[28] K. Arakawa, K. Ono, M. Isshiki, K. Mimura, M. Uchikoshi, and H. Mori, Science **318**, 956 (2007).
[29] Y. Matsukawa and S. J. Zinkle, Science **318**, 959 (2007).
[30] J. Wong-Leung, M. K. Linnarson, B. G. Svensson, and D. J. H. Cockayne, Phys. Rev. B **71**, 165210 (2005).
[31] M. Minor, J. W. Morris, Jr., and E. A. Stach, Appl. Phys. Lett. **79**, 1625 (2001).
[32] D. Skarlatos, P. Tsouroutas, V. Em. Vamvakas, and C. Tsamis, J. Appl. Phys. **99**, 103507 (2006).
[33] Z. Pan, K. N. Tu, and A. Prussin, J. Appl. Phys. **81**, 78 (1997).
[34] V. V. Chaldyshev, A. L. Kolesnikova, N. A. Bert, and A. E. Romanov, J. Appl. Phys. **97**, 024309 (2005).
[35] S. L. Dudarev, R. Bullough, and P. M. Derlet, Phys. Rev. Lett. **100**, 135503 (2008).
[36] F. Lund, J. Mater. Res. **3**, 280 (1988).
[37] T. Mura, Philos. Mag. **8**, 843 (1963).
[38] N. Rodríguez, Tesis de ingeniero, Universidad de Chile, 2008.
[39] The elliptic polarization is often described using Jones polarization vector. $\hat{\mathbf{p}} = \mathrm{Re}\begin{pmatrix} \cos\phi_J; \\ \sin\phi_J e^{i\alpha} \end{pmatrix} e^{i\omega t}$. The correspondence between Jones parameters, the parameters ϕ_J and R, and our ϕ and r is $r = -(R^2+1+\delta)/2R \sin\phi_J$ and $\tan\phi = -(R^2-1+\delta)/2R \cos\phi_J$, with $\delta^2 = (R^2-1)^2 + 4R^2\cos^2\phi_J$.